Electronic structure, chemical bonding, and optical properties of ferroelectric and antiferroelectric NaNO$_2$

P. Ravindran,* A. Delin, B. Johansson, and O. Eriksson

Condensed Matter Theory Group, Department of Physics, Uppsala University, Box 530, 75121 Uppsala, Sweden

J. M. Wills

Theoretical Division, Los Alamos National Laboratory, Los Alamos, New Mexico 87545

The electronic-energy band structure, site and angular momentum decomposed density of states (DOS), and charge-density contours for ferroelectric sodium nitrite have been calculated using an accurate full-potential linear muffin-tin orbital method. The calculated total DOS is found to be in good agreement with experimental x-ray-photoemission spectra. From the DOS analysis, as well as charge-density studies, we conclude that the bonding between Na and NO$_2$ is ionic and that the NO$_2$ entities bond covalently. The polarized reflectivity spectra, calculated in a large energy range up to 30 eV, are directly compared with recent experimental spectra. The optical anisotropy in this material is analyzed through the optical functions such as refractive indices and static dielectric constants along the principal axes. Our calculated band structure and optical spectra are also compared with results obtained from the orthogonalized linear combination of atomic orbital method. The role of antiferroelectric distortion on the optical property and structural stability is discussed. [S0163-1829(99)00503-2]

I. INTRODUCTION

Interactions between alkali metal atoms and simple gas molecules may result in crystals in which the gas molecules become ''frozen in,'' in an ordered way in an array of alkali atoms. One relatively simple example is NaNO$_2$. The result is a highly anisotropic material with several interesting properties such as ferroelectricity and piezoelectricity. Since the discovery of ferroelectricity by Sawada *et al.*[1] in NaNO$_2$, a large number of investigations have been carried out to study its structural changes,[2] its dielectric,[3,4] elastic,[5] electrical,[6] and thermal[7] properties, the infrared (IR), Raman,[8] and nonlinear optical spectra,[9] as well as its nuclear-quadrupole moment.[10] A recent interest in this material stems from the fact that opal, containing regular three-dimensional arrays of nanosized sodium nitrite, shows giant enhancement of the dielectric constant,[11] and hence is of potential interest in connection with applications in ferroelectric memories.

It was found[12] that, upon heating, NaNO$_2$ undergoes a first-order phase transition from ferroelectric to a sinusoidal antiferroelectric phase at the critical point ($T_C = 163.9$ °C), followed by a second-order phase transition to the paraelectric phase at the Neél temperature ($T_N = 165.2$ °C). In the ferroelectric phase NaNO$_2$ has a polar body-centered orthorhombic structure with a C_{2v}^{20} ($Im2m$) space group and is piezoelectric. In the low-temperature phase, all NO$_2^-$ molecules are aligned with the dipoles along the **b** axis of the crystal, which then shows strong optical anisotropy.

In the past, many experimental studies of the optical properties of this material have been performed. Axe[13] measured the infrared reflectivity spectra at room temperature and from this data he calculated the principal dielectric-response functions using the Kramers-Kronig (KK) relations. Hirotsu Yanagi and Sawada[14] measured the temperature dependence

of the principal refractive indices and concluded that the large optical anisotropy arises from the polarizability anisotropy of the nitrite ion. Yamashita and Kato[15] measured the vacuum ultraviolet absorption spectra at room as well as liquid-nitrogen temperatures. Kamada and Kato[16] found a series of vibronic lines accompanied with the phonon side bands in the polarized absorption spectra. Kawaura, Kawaguchi, and Kato[17] studied the characteristics of the lowest singlet exciton in NaNO$_2$ using high-resolution measurements of reflection spectra at 2 K. Most of these studies, however, concentrated on the far IR region of the spectrum. To our knowledge, the only exception is the very recent paper by Ashida *et al.*,[26] who measured the polarized reflectivity spectra for NaNO$_2$ at room temperature, as well as liquid-nitrogen temperature for a very wide energy range up to 25 eV.

Also, quite a few theoretical investigations of the band structure and optical properties of NaNO$_2$ have been reported. NaNO$_2$ has one of the simplest crystal structures among ferroelectrics. Hence, information regarding its electronic structure may prove very useful in studies of phase transitions in ferroelectrics. The electronic-energy band structure of ferroelectric NaNO$_2$ was first calculated by Kam and Henkel[3] using an X_α exchange and a mixed plane-wave Gaussian basis set. El-Dib and Hassan[20] calculated the temperature dependence of the electronic-energy bands of this material using a semiempirical linear combination of atomic orbitals (LCAO) method from the temperature-dependent lattice parameters measured by Kucharczyk *et al.*[21] and the atomic coordinates given by Kay and Frazer.[22,23] From this study they found that the band gap increases almost linearly with temperature, and also that the general features of the bands at various temperatures are similar to those at 20 °C. Using the self-consistent orthogonalized linear combinations

of atomic orbitals (OLCAO) method, Jiang, Xu, and Ching[24] calculated the electronic structure and dielectric function. Zhong, Jiang, and Ching[25] studied the effect of disorder on the optical properties of paraelectric $NaNO_2$ and found that disorder decreases the optical anisotropy, bandgap, and the value of the dielectric function. Wyncke, Bréhat, and Kharoubi[18] calculated the reflectivity as a function of the angle of incidence and compared it with experimental results. $NaNO_2$ is also a nonlinear optical crystal and Wu and Chen[19] made *ab initio* molecular-orbital calculations to study the origin of birefringence in this material. However, no theoretical study of this compound have been performed using a first-principles full-potential method. Since the crystal structure of $NaNO_2$ is open and the calculated properties rely critically on accurate eigenvalues and eigenvectors, the use of a full-potential method is essential in order to achieve accurate theoretical dielectric functions.

The rest of this paper is organized as follows. Crystal-structural aspects and computational details regarding the method used in our calculations of the electronic structure and optical properties are described in Sec. II. Section III deals with the band structure and density of states of $NaNO_2$. In this section we also explain the chemical bonding in this material by analyzing the charge density and the angular momentum and site-decomposed density of states. The band structure and the optical properties obtained from our calculations are given in Sec. IV, where they are compared it with available experimental results. The conclusions we draw from the present studies are summarized in Sec. V.

II. STRUCTURAL ASPECTS AND COMPUTATIONAL DETAILS

The crystal structure of $NaNO_2$ in the ferroelectric and paraelectric phases have been studied experimentally using x-ray[27] and neutron-scattering techniques.[28,29] The ferroelectric phase considered here is body-centered orthorhombic (C_{2v}^{20} space symmetry). It belongs to the space group $Im2m$ and contains two molecules per cell. In the unit cell, the two Na atoms are located at the Wycoff $2a$ site (0 0 0.5862), the two N atoms are at the $2a$ site (0 0 0.1188), and the four O atoms are at the $4d$ site (0 0.1944 0). We have used the lattice parameters $a = 3.55$, $b = 5.38$, and $c = 5.56$ Å and the above atomic-positional parameters taken from the single crystal x-ray diffraction measurements of Carpenter.[30] Figure 1(a) shows the orthorhombic unit cell of the $NaNO_2$ crystal in the ferroelectric phase. The crystallographic axes used in our optical property studies are denoted as shown in this figure. The antiferroelectric phase displays a sinusoidal modulation along the $i\mathbf{a}$ axis with a period of about $8a$.[31] For our antiferroelectric calculations, even though $NaNO_2$ possesses a sinusoidal antiferroelectric phase, for simplicity we have only considered a commensurate antiferroelectric phase of the type shown in Fig. 1(b).

The full-potential linear muffin-tin orbital (FPLMTO) calculations[32] presented in this paper are all electron, and no shape approximation to the charge density or potential has been used. The base geometry in this calculational method consists of a muffin-tin part and an interstitial part. The basis set was comprised of augmented linear muffin-tin orbitals.[33] Inside the muffin-tin spheres the basis functions, charge den-
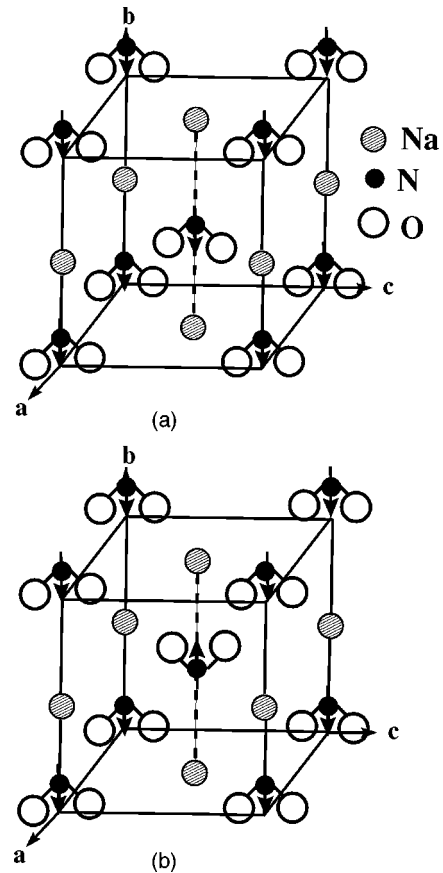
FIG. 1. The unit cell of $NaNO_2$ in the body-centered orthorhombic structure. $\mathbf{a}$, $\mathbf{b}$, and $\mathbf{c}$ are the crystallographic axes used for optical property studies. (a) The ferroelectric phase. (b) Antiferroelectric phase.

sity, and potential are expanded in symmetry-adapted spherical-harmonic functions together with a radial function. In the present calculation the spherical-harmonic expansion of the charge-density, potential, and basis functions were carried out up to $\ell_{max} = 6$. The tails of the basis functions outside their parent spheres are linear combinations of Hankel and Neuman functions. For numerical reasons, these basis functions in the interstitial are represented as the Fourier series. For the core charge density, the Dirac equation is solved self-consistently, i.e., no frozen-core approximation is used. The calculations are based on the local-density approximation to the density-functional theory with the exchange-correlation potential parametrized according to Hedin and Lundquist.[34] The completeness of the basis set, with different variational κ values for each partial wave in the interstitial region, allows the method to treat open structures such as that of $NaNO_2$, without having to resort to the use of so-called empty spheres. The volume ratio between the interstitial region and the unit cell is approximately 0.758 in the present calculations. The $\mathbf{k}$-space integration was performed using the special-point method[35] with 1000 irreducible $\mathbf{k}$ points in the whole Brillouin zone for the self-consistent ground-state calculations and 15 625 $\mathbf{k}$ points for our optical studies. The irreducible $\mathbf{k}$ points were obtained by shifting the $\mathbf{k}$-space grid away from the high-symmetry planes and the Γ point by a half step in each of the k_x, k_y, and k_z directions. This scheme produces highly accurate integration

in the Brillouin zone, using a smaller amount of **k** points than would be necessary if high-symmetry **k** points are included. To ensure the **k**-point convergence regarding the optical properties we have also carried out studies using 8000 **k** points. The optical spectra obtained from 15 625 **k** points as well as 8000 **k** points are essentially the same. In the antiferroelectric phase calculations we have used 768 **k** points for the self-consistent ground-state calculations and 6656 **k** points for the optical-property studies.

The tight-binding LMTO method with atomic-sphere approximation (TBLMTO-ASA) calculation of the basis set consists of sodium $3s$, nitrogen $2s$ and $2p$, oxygen $2s$ and $2p$, and the empty sphere $1s$ LMTO's. The sodium $3p$ and $3d$, nitrogen $3d$, oxygen $3d$, and the empty spheres $2p$ and $3d$ partial waves were included in the tails of the above-mentioned LMTO's. In order to achieve the overlap between the spheres to be less than 20%, we have included two empty spheres in 0 0.5 0.39728 and 0.5 0 0.51213 positions in the primitive cell. Though the TBLMTO-ASA method is not accurate compared with the FPLMTO method, due to its physically transparent nature we have used this method for our analysis.

The calculation of optical properties requires, apart from the Kohn-Sham eigenvalues, the explicit use of the wave functions, which, therefore, should be described as accurately as possible. In the computational method used here, we have gone beyond a minimal basis set using a so-called double basis. Three different kinetic energies were used for each subset of s and p derived bases in the basis set; two kinetic energies were used for bases derived from orbital parameters $\ell > 1$. The basis sets used in calculating the electronic structure and optical properties were, for Na ($2p, 3s, 3p,$ and $3d$), for N ($2s, 2p,$ and $3d$), for O ($2s, 2p,$ and $3d$). A useful feature of the method used in these calculations is the ability to incorporate basis functions derived from the same orbital-atomic quantum numbers by different principal atomic quantum numbers in a single fully hybridizing basis set. This feature entails the use of multiple sets of radial functions to represent bases with different principal atomic quantum numbers. This capability was particularly useful in calculating the high-lying energy bands that were used to obtain the dielectric functions at high energies.

A. Optical properties

The linear response of a system due to an external electromagnetic field with a small wave vector can be described with the complex dielectric function $\epsilon(\omega) = \epsilon_1(\omega) + i\epsilon_2(\omega)$. We have calculated the dielectric function for frequencies well above those of the phonons, and, therefore, we considered only electronic excitations. For these we used the random-phase approximation,[36] neglecting local-field and finite lifetime effects. Moreover, due to the orthorhombic structure of $NaNO_2$ the dielectric function is a tensor. By an appropriate choice of the principal axes we could diagonalize it and restrict our considerations to the diagonal matrix elements. The interband contribution to the imaginary part of the dielectric functions $\epsilon_2(\omega)$ is calculated by summing transitions from occupied to unoccupied states (with fixed **k** vector) over the Brillouin zone, weighted with the appropriate matrix element giving the probability for the transition. To be specific, the components of $\epsilon_2(\omega)$ are given by

$$\epsilon_2^{ij}(\omega) = \frac{Ve^2}{2\pi\hbar m^2\omega^2} \int d^3k \sum_{nn'} \langle \mathbf{k}n|p_i|\mathbf{k}n'\rangle\langle \mathbf{k}n'|p_j|\mathbf{k}n\rangle$$
$$\times f_{\mathbf{k}n}(1-f_{\mathbf{k}n'})\,\delta(\epsilon_{\mathbf{k}n'} - \epsilon_{\mathbf{k}n} - \hbar\omega). \quad (1)$$

Here $(p_x, p_y, p_z) = \mathbf{p}$ is the momentum operator, $f_{\mathbf{k}n}$ is the Fermi distribution, and $|\mathbf{k}n\rangle$ the crystal wave function, corresponding to energy eigenvalue $\epsilon_{\mathbf{k}n}$ with crystal momentum **k**. The evaluation of matrix elements in Eq. (1) is done over the muffin-tin and interstitial regions separately. Further details about the evaluation of matrix elements are given elsewhere.[37] We have calculated the three components $\mathbf{E}\|\mathbf{a}$, $\mathbf{E}\|\mathbf{b}$, and $\mathbf{E}\|\mathbf{c}$ of the dielectric constants corresponding to the electric field parallel to the crystallographic axes **a**, **b**, and **c**, respectively. The calculations yield the unbroadened functions. To reproduce the experimental conditions correctly, it is necessary to broaden the calculated spectra. The exact form of the broadening function is unknown, although comparison with measurements suggests that the broadening usually increases with increasing excitation energy. Also, the instrumental resolution smears out many fine features. To simulate these effects the lifetime broadening was simulated by convoluting the absorptive part of the dielectric function with a Lorentzian, whose full width at half maximum (FWHM) is equal to 0.01 eV at the photon energy 1 eV, and increasing quadratically with the photon energy. The experimental resolution was simulated by broadening the final spectra with a Gaussian, where the FWHM is equal to 0.02 eV. The real part of the components of the dielectric tensor $\epsilon_1(\omega)$ are then calculated using the Kramer-Kronig transformation. The knowledge of both the real and imaginary parts of the dielectric tensor allows the calculation of important optical constants. In this paper, we present and analyze the reflectivity $R(\omega)$, the absorption coefficient $I(\omega)$, the electron energy-loss spectrum $L(\omega)$, as well as the refractive index n and the extinction coefficient k. The reflectivity spectra are derived from the Fresnel's formula for normal incidence assuming an orientation of the crystal surface parallel to the optical axes using the relation

$$R(\omega) = \left|\frac{\sqrt{\epsilon(\omega)} - 1}{\sqrt{\epsilon(\omega)} + 1}\right|^2. \quad (2)$$

We calculated the absorption coefficient $I(\omega)$ and the electron energy-loss spectrum $L(\omega)$ using the following expressions:

$$I(\omega) = 2\omega\left(\frac{[\epsilon_1^2(\omega) + \epsilon_2^2(\omega)]^{1/2} - \epsilon_1(\omega)}{2}\right)^{1/2}, \quad (3)$$

$$L(\omega) = \frac{\epsilon_2(\omega)}{\epsilon_1^2(\omega) + \epsilon_2^2(\omega)}. \quad (4)$$

The refractive index n and the extinction coefficient k were obtained by the following formulas:

$$n = \left(\frac{\sqrt{\epsilon_1^2 + \epsilon_2^2} + \epsilon_1}{2}\right)^{1/2}, \quad (5)$$
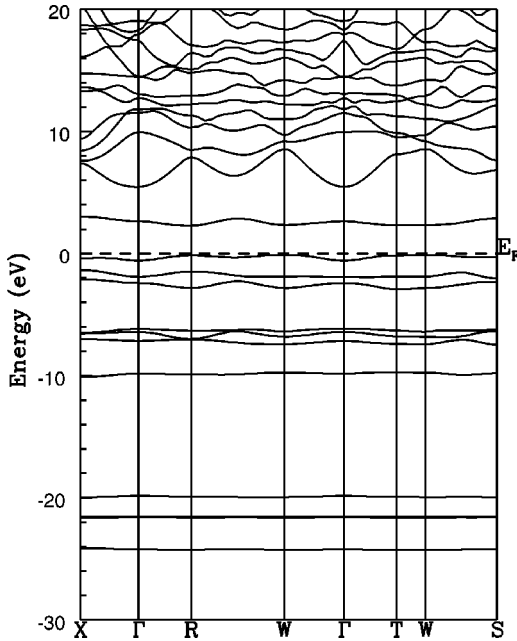
FIG. 2. Calculated energy-band structure of $NaNO_2$. The energy of the top of the valence band is set to zero.

$$k = \left(\frac{\sqrt{\epsilon_1^2 + \epsilon_2^2} - \epsilon_1}{2} \right)^{1/2}. \tag{6}$$

III. RESULTS: GROUND-STATE ELECTRONIC STRUCTURE

A. Band-structure results

Since the optical spectra are calculated from interband transitions, it is of interest to first describe our calculated electronic structure. For this reason, the calculated band structure of ferroelectric $NaNO_2$ in the high-symmetry directions in the Brillouin zone are shown in Fig. 2. From this figure it is clear that the bands have little dispersion, which is typical of a molecular solid. This is also consistent with previous studies.[24] An interesting feature of this band structure is the presence of a very flat band in the topmost valence band (VB) as well as the bottommost conduction band (CB), which is separated from the rest of the bands by a wide gap.

There are 12 bands in the valence region shown in Fig. 2. The lowest-lying valence band consists of three degenerate bands around -27.5 eV, and arises from the Na $2p$ orbitals. Due to the hybridization between $2s$ states of oxygen and nitrogen a single band forming around -24 eV and this has bonding character. Above this band, there is one localized band around -20 eV, arising mainly from oxygen $2s$ orbitals with considerable nitrogen p_y character. In the present analysis we have chosen the x, y, and z axes, which are the a, b, and c crystallographic axes defined in Fig. 1(a), respectively. The single band at ~ 10 eV consists of oxygen $2s$ states as well as nitrogen $2s$ states in almost equal amounts. This band is having the anti-bonding character arising from the covalent hybridization of oxygen $2s$ with the nitrogen $2s$ states. The three bands in the -8.5 eV range have pure p character and correspond to ~ 2 nitrogen $2p$ (mainly p_x and p_y character) electrons and ~ 4 oxygen $2p$ electrons (mainly
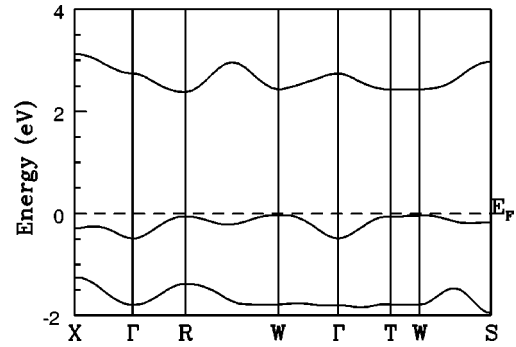
FIG. 3. Calculated energy-band structure of $NaNO_2$ in the vicinity of the fundamental absorption edge. Note that the fundamental gap is between the VB maximum at W and the CB minimum at R. The energy of the top of the valence band (E_F) is set to zero.

having p_x and p_y character, with the bottom band containing a slight p_z character). The top of the valence region contains three bands in which the bottommost two bands arise purely from the oxygen $2p$ orbitals. A detailed analysis shows that they have p_x and p_y oxygen character. The topmost valence band mainly has the bondinglike phase relationship between the oxygen and nitrogen p_z orbitals with a small contribution from sodium and nitrogen s electrons. The corresponding antibonding hybrid is in the unoccupied state and not discussed in detail here.

Since the bands in the topmost valence band and bottommost conduction bands are very flat, it is difficult for the eye to identify the maximum in the valence band and the minimum in the conduction band directly from Fig. 2. Therefore, we have given the band structure of $NaNO_2$ in an expanded energy scale around the energy gap in Fig. 3. From this figure it is clear that the band gap appears between the topmost VB at W and the bottom most CB at R. Our calculated value of the indirect band gap is 2.2 eV, which is smaller than the value 2.95 eV obtained from the OLCAO method by Jiang, Xu, and Ching.[24] Further, they obtain the VB maximum at S, which is different from our result. To clarify this issue we have repeated our calculations using the TBLMTO method in the atomic-sphere approximation. We find that irrespective of the band-structure method used, the fundamental gap lies between the VB maximum at W and the CB minimum at R. Our calculated fundamental gap is smaller than the experimentally reported values of 3.14 eV (Ref. 38) and 3.22 eV,[39] as it should be because of the discontinuity in the exchange-correlation potential, which is not taken into account here.

B. Density of states and chemical bonding

Our calculated total density of states (DOS) curve for $NaNO_2$ along with the experimentally reported[40] x-ray photoemission spectroscopy (XPS) spectrum are shown in Fig. 4. Our DOS exhibits sharper peaks than the experimental spectra, since we have not included the lifetime broadening and instrumental resolution in our DOS curve. To get more insight into the valence-band spectra near E_F, we show the angular momentum and site decomposed DOS on a more expanded energy scale in Fig. 5. In this figure, we see that the Na states are high up in the CB at about 5 eV above E_F, indicating a nearly total ionization of the Na atom. The nar-
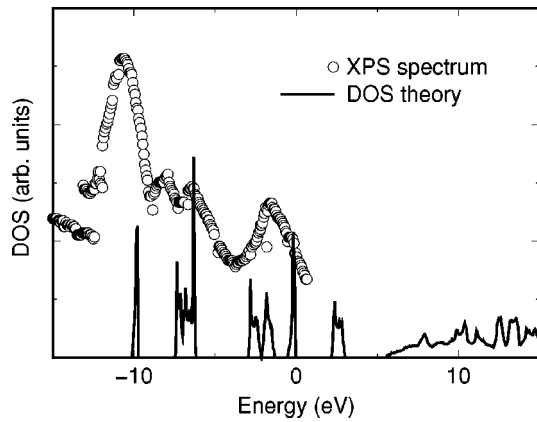
FIG. 4. The calculated total DOS curve is compared with the XPS spectrum reported by Kamada, Ichikawa, and Tsutsumi (Ref. 40). No shifting of the XPS spectrum relative to the DOS has been performed. The energy of the top of the valence band is set to zero.

row impuritylike CB about 1 eV wide is the result of hybridization between N $2p$ and O $2p$ orbitals. The highest VB is only 0.75 eV wide and involves mainly O $2p$, N $2p$, and Na $3s$ orbitals. Slightly below this peak, in the VB DOS around -2.5 eV, there is a peak arising purely from the O $2p$ orbitals.
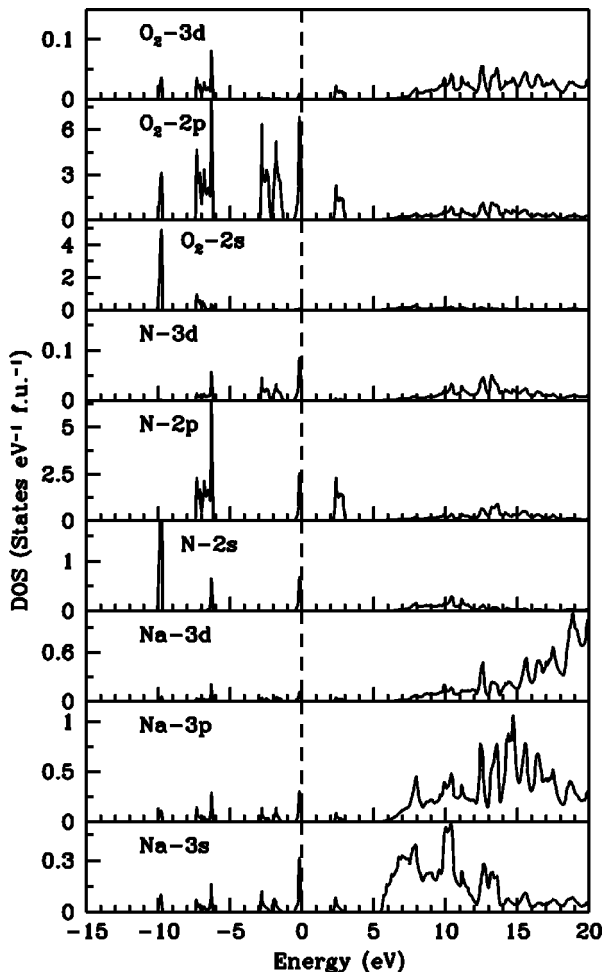
FIG. 5. The angular momentum and site-projected density of states of NaNO$_2$. The energy of the top of the valence band is set to zero.
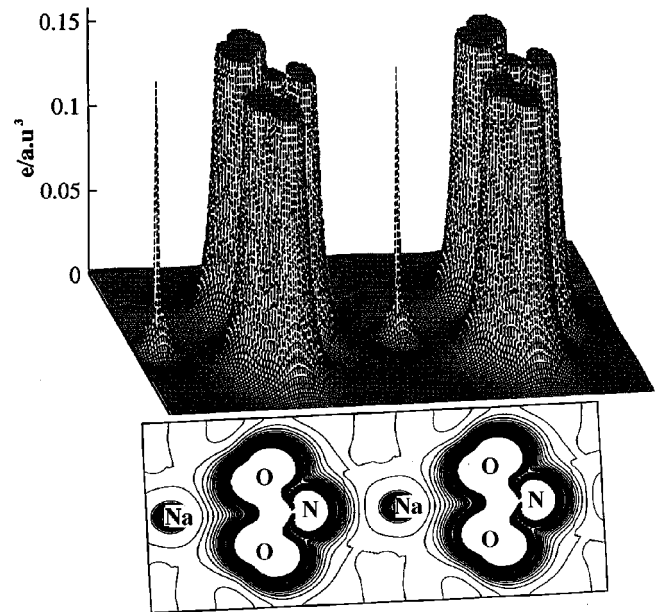
FIG. 6. The valence charge-density contour of ferroelectric NaNO$_2$ in the (100) plane. 90 contours are drawn between 0.01 and 0.1 electrons/a.u.^{3} A three-dimensional plot of the same is in the upper panel.

In order to understand the chemical bonding in more detail, we show in Fig. 6 the charge density of NaNO$_2$ in the *bc* plane of the ferroelectric phase. The experimental linear compressibility study on NaNO$_2$ show that the compression perpendicular to rigid N-O bonds is approximately 3.5 times greater than compression within the plane of N-O bonding.[41] This shows the presence of anisotropic bonding behavior in this material and also indicates a strong bonding between nitrogen and oxygen in NaNO$_2$. Further the interatomic distance between the N and O is only 1.237 Å, and that between Na and O is 2.598 Å indicating that the bonding between nitrogen and oxygen is covalent in nature. Sodium nitrite has been described as distorted NaCl-type arrangements of Na$^+$ and NO$_2^-$ groups.[42] Alkali halides with the NaCl structure demonstrate an inverse relationship between molar volume (V) and bulk modulus (K). $KV = 11.3 \pm 0.5$ Mbar Å^3. Hazen and Finger[41] found that this correlation holds good ($KV = 11.7$) for NaNO$_2$, indicating that it can be viewed as ionic NaCl-like material. In support of this viewpoint our calculated total valence charge in the Na muffin-tin sphere is found to be less than 0.1 electrons. Further, the more electropositive nature of Na compared with N and O confirm the presence of ionic bonding between Na and NO$_2$. The negligible charge density between Na and NO$_2$, as well as the very low-electron population at the Na site, much lower than for a neutral Na atom, is a clear indication of the ionic bonding between Na and NO$_2$. Hence, the NO$_2$ as a whole can be viewed as a negatively charged unit. To show the bonding within this unit more clearly, we have also plotted the corresponding three-dimensional charge-density map in the upper panel in Fig. 6. From this figure it is clearly evident that substantial covalent bonding exists between nitrogen and oxygen. Okuda *et al.*[43] studied the bonding behavior of NaNO$_2$ by an oriented-atom model with multipole expansion and found σ-type bonding between N and O originating from
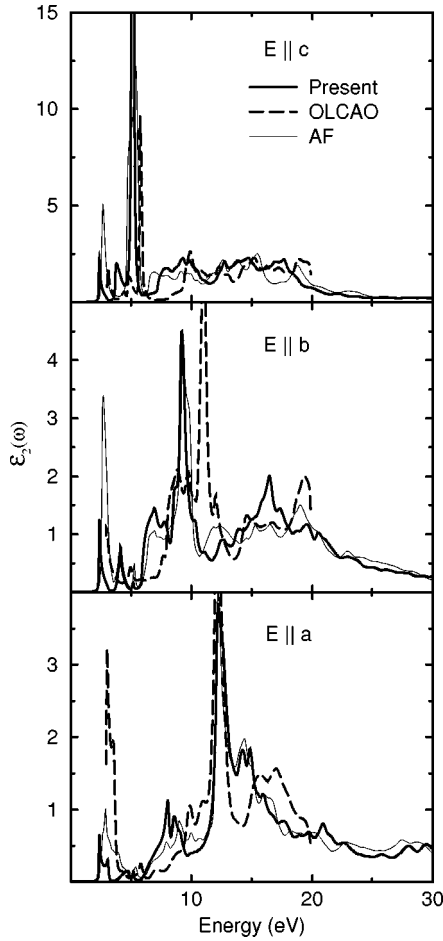
FIG. 7. Calculated components of $\epsilon_2(\omega)$ along the crystallographic axes. The OLCAO results are taken from Jiang, Xu, and Ching (Ref. 24). The bold continuous line represents the ferroelectric phase and the thin continuous line represents the antiferroelectric phase.

sp^2 hybridization. This is consistent with our observation of covalent bonding between nitrogen and oxygen in $NaNO_2$. The observed large-bonding anisotropy in $NaNO_2$ (i.e., ionic bonding between Na and NO_2 and a strong covalent bond between N and O) is likely the principal cause for the experimentally observed large anisotropy in linear compressibilities.[41] Our total energy calculations show that the antiferroelectric phase is found to be around 9 mRy/f.u. higher in energy than the ferroelectric phase. This is consistent with the experimental studies, since the ferroelectric phase is stable at lower temperatures.

IV. RESULTS: OPTICAL PROPERTIES

Further insight into the electronic structure can be obtained from the calculation of interband optical functions. The optical properties of $NaNO_2$ are very anisotropic, and therefore we resolve the optical spectra into the three principal directions $\mathbf{E}\|\mathbf{a}$, $\mathbf{E}\|\mathbf{b}$, and $\mathbf{E}\|\mathbf{c}$, corresponding to the electric-field vector polarized along the crystallographic axis $\mathbf{a}$, $\mathbf{b}$, and $\mathbf{c}$, respectively. The calculated imaginary part of the dielectric function for $NaNO_2$ along the $\mathbf{a}$, $\mathbf{b}$, and $\mathbf{c}$ axes of the crystal are shown in Fig. 7 along with those obtained by Jiang, Xu, and Ching using the OLCAO method.[24] Overall,

the dielectric spectra obtained from these computationally very different band-structure methods are seen to be consistent with each other. The main discrepancy in the dielectric spectra between the present results and the OLCAO results is for the spectrum with electric-field vector polarized along the crystallographic axis $\mathbf{a}$. In the lower energy peak, our calculation gives a maximum value less than 1. But the reported[24] OLCAO maximum value is greater than 3. Further, we observe a peak structure around 9 eV in our $\epsilon_2(\omega)$ $\mathbf{E}\|\mathbf{a}$ spectra, which is well separated from the main peak around 12 eV. In the OLCAO results, this peak shows up as a shoulder in the main peak.

Since the optical spectra are obtained from the interband transitions, the peak structures in Fig. 7 can be explained through our band structure. The lowest-energy peak at 2.2 eV in the $\epsilon_2(\omega)$ spectra in $\mathbf{E}\|\mathbf{a}$, $\mathbf{E}\|\mathbf{b}$, and $\mathbf{E}\|\mathbf{c}$ arises from the interband transition between the topmost valence band and the bottommost conduction band (i.e., band 12 → band 13). Around 4 eV a peak appears in all three directions. The origin of this peak is due to band 11 → band 13 interband transitions. A sharp peak around 5.2 eV in the $\mathbf{E}\|\mathbf{c}$ spectrum originates from band 10 → band 13 interband transitions. This peak is absent in the $\mathbf{E}\|\mathbf{a}$ and $\mathbf{E}\|\mathbf{b}$ spectra. Overall, the dielectric function exhibits large anisotropy in this material. The peak structure around 9.15 eV in the $\mathbf{E}\|\mathbf{b}$ spectrum mainly arises from the combination of 8→13, 10→14, and 12→15 interband transitions, and the peak at 12.14 eV arises mainly from 6→13 interband transition with small contributions coming from 8→14, 9→14, 10→16, and 11→16 interband transitions. The peaks in the $\epsilon_2(\omega)$ spectra above 10 eV, visible in all three directions, are broad and involve several bands.

Newman[44] deduced the values of the dielectric constant for infinite wavelength to be 1.818, 1.99, and 2.77 along the crystallographic $\mathbf{a}$, $\mathbf{b}$, and $\mathbf{c}$ axes, respectively. This can be interpreted as due to electronic polarization without the effect of lattice vibrations at the low-frequency end. Our calculated $\epsilon_1(0)$ values along $\mathbf{a}$, $\mathbf{b}$, and $\mathbf{c}$ are 1.97, 2.27, and 3.98, respectively, values that compare favorably with the corresponding experimental values mentioned above. Thus, $\epsilon_1(0)$ is rather well described using vertical interband transitions only. However, theory predicts more anisotropy in the optical properties of $NaNO_2$ than experiment. Jiang, Xu, and Ching also reported calculated $\epsilon_1(0)$ values along the principal axes. Their values are 1.58, 1.60, and 2.20 for polarization along the $\mathbf{a}$, $\mathbf{b}$, and $\mathbf{c}$ principal axes, respectively.

From our calculation the calculated value of the fundamental gap in the antiferroelectric phase is 2.116 eV. In order to understand the role of antiferroelectric distortion on the optical properties on $NaNO_2$, we have also given the $\epsilon_2(\omega)$ spectra for the antiferroelectric phase along all the three crystallographic axes in Fig. 7. Except for the absolute values, overall the peak positions of both ferroelectric and antiferroelectric phases are consistent with each other.

In Fig. 8 we compare our calculated reflectivity spectra with experimental[26] polarized-reflectivity spectra. We have also generated theoretical-reflectivity spectra for $NaNO_2$ by KK, transforming the $\epsilon_2(\omega)$ spectra reported by Jiang *et al.*[24] calculated using the OLCAO method. Overall, our theoretical spectra are found to be in good agreement with experiments above 8 eV. The good agreement between ex-
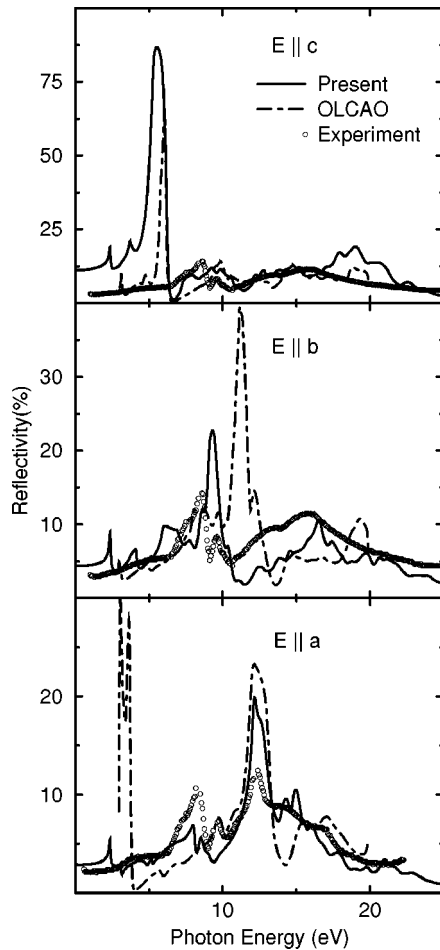
FIG. 8. Polarized reflectivity spectra for $NaNO_2$. The circles represent data taken from the experimental studies by Ashida *et al.* (Ref. 26). The dashed lines are the reflectivity spectra calculated from the $\epsilon_2(\omega)$ spectra reported by Jiang *et al.* (Ref. 24) by KK transformation. No shift of the energy scale is involved.

periment and theory in the higher-energy range indicates high accuracy of our unoccupied states. The main discrepancies between the experimental reflectivity spectra of Ashida *et al.*[26] and theory reside below 5 eV. Our theoretical spectra show peak structures at lower energies, which are absent in the experimental spectra. As mentioned earlier, the present study and the results reported by Jiang, Xu, and Ching[24] show a sharp peak in the $\epsilon_2(\omega)$ spectra at $\mathbf{E}\|\mathbf{c}$ around 5 eV. This peak gives rise to a peak structure in our $\mathbf{E}\|\mathbf{c}$ reflectivity spectra in Fig. 8 in the same energy range. It is interesting to note that although both theoretical studies show large reflectivity around 5 eV in the $\mathbf{E}\|\mathbf{c}$ direction, the experimental spectra of Ashida *et al.*[26] do not show this feature. Our calculated $\epsilon_2(\omega)$ spectra for the antiferroelectric phase also show a sharp peak around 5 eV in the $\mathbf{E}\|\mathbf{c}$ direction. We hope that the present theoretical observations will motivate further experimental studies in this energy range. Our calculated reflectivity spectra differ considerably from the calculated reflectivity spectra of Jiang, Xu, and Ching[24] for $\mathbf{E}\|\mathbf{a}$ but agree much better with experimental data. This difference illustrates that a theoretical description of the dielectric response depends on the accuracy of the method.

There is no simple explanation for the remaining discrepancies between experimental reflectivity spectra and theory

in Fig. 8. Their main origin may well be the local-density approximation. The formalism of density-functional theory (DFT) is in principle exact for ground-state properties. However, even for the exact DFT the one-particle spectrum of the noninteracting reference system may differ from the spectrum of the actual one-electron excitations (OEE) in a solid, obtained in the optical measurements. As discussed by Bellani *et al.*,[45] the OEE spectrum, defined by the poles of the one-particle Green function, is given by the Dyson-type equation containing the self-energy operator $\Sigma_{xc}(r,r',E)$ instead of the local exchange-correlation potential V_{xc} in DFT. The self-energy operator is nonlocal and is also energy dependent. Particularly, for the well-localized molecular solid such as $NaNO_2$, the poor screening of the exchange interaction makes Σ_{xc} more nonlocal than in metals. Further, the discrepancies in the reflectivity spectra between experiment and theory is not only a consequence of the limited accuracy of the theoretical and numerical treatments. The sample quality, the surface treatment, the sample size, and the technical difficulties of handling the radiation source may influence the reflectivity spectra. Moreover, the experimentally reported reflectivity spectra were obtained by adjusting the observed reflectivity spectra so as to fit to the values estimated from the refractive indices n_a, n_b, and n_c, respectively, in the visible region.

Kamada, Yoshikawa, and Kato[46] measured the polarized UV absorption spectra of $NaNO_2$ at low temperatures and found phonon sidebands in the spectrum. Our calculated absorption spectra $I(\omega)$ is shown in the lowest panel of Fig. 9. It should be emphasized that the present calculation of the dielectric function only pertains to the electronic response, and does not include the effects of lattice vibrations that dominate the experimental absorption spectrum in the low-frequency region. Therefore, we can naturally not expect the experimentally observed[16,46,47] series of vibronic lines accompanying the phonon sidebands in the absorption spectrum given in Fig. 9. Unfortunately, experimental polarized-absorption spectra for $NaNO_2$ are available only for the energy range 0–4 eV. This, and the fact that the experimental absorption spectra are dominated by the phonon contributions, make a comparison between our calculated spectra and the existing experimental studies rather meaningless. However, as our theoretical absorption spectra contains purely the electronic contribution, it may prove useful as a reference in future experimental studies.

We now proceed to a more detailed analysis of the peaks in the $I(\omega)$ spectra. According to molecular-orbital calculations by McEwen,[48] the UV absorption at 3.5 and 4.2 eV in $NaNO_2$ are interpreted as the intramolecular electronic transitions of NO_2^-. Yamashita and Kato[15] observed three characteristic peaks in the absorption spectrum of thin film $NaNO_2$, one at 6.1 eV, a second at 9.6 eV, and the third at 11 eV. From our theoretical absorption spectra given in Fig. 9, it is clearly evident that the 6.1-eV peak (in our case at 5.2 eV) originates from absorption in the $\mathbf{E}\|\mathbf{c}$ direction, whereas the other two peaks arise from absorption in all three crystallographic directions. Experimental studies[15] show that the 6.1-eV absorption peak does not shift if Na is replaced by K. Hence, it is interpreted as originating from electronic excitations in the anions. Our detailed analysis of the absorption spectra show that the origin of this peak is due to the band
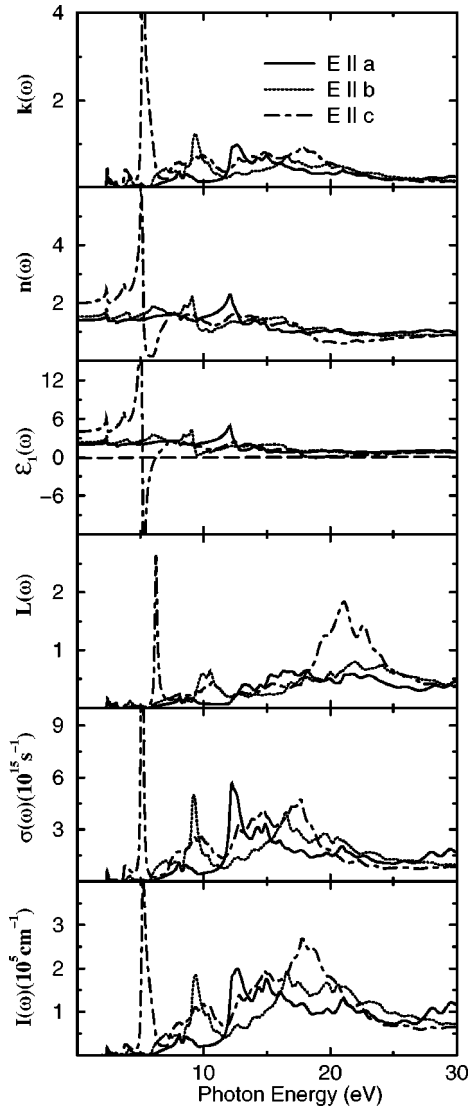
FIG. 9. The calculated absorption coefficient $[I(\omega), 10^5 \text{ cm}^{-1}]$, optical conductivity $[\sigma(\omega)]$, electron energy-loss function $[L(\omega)]$, real part of dielectric constant $[\epsilon_1(\omega)]$, the refractive index $[n(\omega)]$, and extinction coefficient $[k(\omega)]$ along the principal axes.

$10 \rightarrow 13$ interband transition. As the bottommost valence band contains a considerable amount of $O(3d)$ states, this peak thus arises from the O $2p$ to O $3d$ interband transition. The peaks around 10 eV are due to N,O$(2p) \rightarrow$ Na$(3s)$ interband transitions. This is consistent with experimental results[15] in the sense that the position of this peak shifts considerably if one replaces Na by K in NaNO$_2$ in the experimental measurements. For clarity, we state explicitly that notation such as O$(2p) \rightarrow$ Na$(3s)$ does absolutely not imply that the optical transition takes place from one atomic site to another. All orbitals have tails extending into the neighboring spheres, and it is in this way that the optical transitions may take place.

Refractive indices of a crystal are closely related to the electronic polarizability of ions and the local field inside the crystal. Another interesting point connected with the refractive indices is the electro-optic effect. Especially in ferroelectrics, spontaneous polarization induces the spontaneous electro-optic effect in the ferroelectric phase. We have given the polarized refractive indices $n(\omega)$ in the second panel of

Fig. 9. From these we have calculated the low-frequency refractive index along the **a**, **b**, and **c** crystallographic axes and obtained the values $n_a = 1.407$, $n_b = 1.507$, and $n_c = 1.995$. These values compare favorably with the room-temperature experimental values[14] $n_a = 1.3455$, $n_b = 1.4125$, and $n_c = 1.6547$. Among these values n_c deviates the most from the experiment. A possible explanation is that this is due to a temperature effect. Experimental studies[14] show that n_a and n_b are almost temperature independent, whereas n_c increases with decreasing temperature. As our theoretical results are valid only for lower temperatures, more experimental studies at very low temperatures are needed for a more meaningful comparison. The polarized refractive-index spectra given in the second part of Fig. 9 resemble the real part of the dielectric tensor in a wide-frequency range from the red-spectral region. It should be noted that the light polarized parallel to the **c** axis is more refracted than that with polarization along the **a** and **b** axes. This clearly indicates the large-optical anisotropy in NaNO$_2$. The observed anisotropy in the refractive index is consistent with experimental observations[14] in the sense that the $n_c - n_a$ value at low temperature is around five times larger than $n_a - n_b$.

The theory also predicts a strong anisotropy of the polarized $\epsilon_1(\omega)$ spectra (see the third panel in Fig. 9). The sign changes occur in the $\epsilon_1(\omega)$ spectra at 5.12 eV in $\mathbf{E} \| \mathbf{c}$ and 9.45 eV in $\mathbf{E} \| \mathbf{b}$ and they appear at the same energy as a peak in the corresponding $\epsilon_2(\omega)$ spectra. Since in this range the imaginary part of the dielectric function is very low, the conditions for a plasma resonance are satisfied. Hence, there are strong resonance maxima at these energies in the calculated energy-loss spectra $L(\omega)$ for these polarizations, as can be seen in the fourth panel of Fig. 9. As the optical conductivity and extinction coefficients are often measured experimentally, those optical functions are also given in Fig. 9.

Since the optical properties of NaNO$_2$ are highly anisotropic, it is particularly interesting to calculate the effective number of valence electrons per NaNO$_2$ molecule n_{eff} contributing to the optical properties in each direction. This can be accomplished by means of the sum rule[48]

$$n_{\text{eff}}(E_m) = \frac{2m}{Ne^2 h^2} \int_0^{E_m} E \epsilon_2(E) dE, \qquad (7)$$

where E_m denotes the upper limit of integration. The quantities m and e are the electron mass and charge, respectively. N stands for the electron density. The effective number of valence electrons per NaNO$_2$ participating in the interband transitions along the crystallographic directions are shown in Fig. 10. The $n_{\text{eff}}(E_m)$ curve of NaNO$_2$ exhibits higher absolute values for $\mathbf{E} \| \mathbf{c}$ than for $\mathbf{E} \| \mathbf{a}$ and $\mathbf{E} \| \mathbf{b}$. This is connected to the large reflectivity feature observed in the $\mathbf{E} \| \mathbf{c}$ at the lower-energy range. Furthermore, as seen from Fig. 10, $n_{\text{eff}}(E_m)$ does not reach a saturation value below 30 eV. This shows that the deep-lying valence orbitals participate in the interband transition.

V. SUMMARY

We have made a detailed investigation of the electronic structure and optical properties of ferroelectric NaNO$_2$ using the full-potential LMTO method. Our FLMTO, as well as
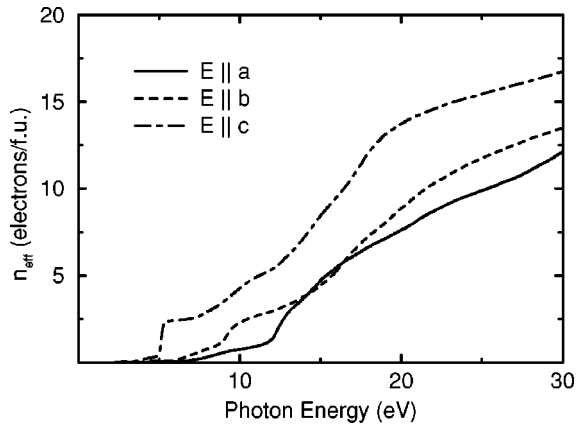
FIG. 10. The calculated effective number of electrons (n_{eff}) participating in the interband optical transitions along the principal axes.

TBLMTO calculations show that the fundamental gap of $NaNO_2$ is indirect with the maximum of the topmost valence band situated at W and the minimum of bottommost conduction band situated at R. Using the ℓ-projected density of states and band structure we have analyzed the interband contribution to the optical properties. The chemical bonding of $NaNO_2$ is also analyzed. The NO_2 complex is bonded by covalent bonds and the Na and NO_2 constituents are bonded ionically. In addition, we find that the ferroelectric phase is lower in energy, compared to an antiferroelectric phase. This is in agreement with observation.

Our calculations indicate strong bonding anisotropy be-tween the constituents of $NaNO_2$. The polarized-reflectivity spectra obtained from our first-principles calculations are found to be in good agreement with the experimental results of Ashida *et al.*[26] above 5 eV. We have examined the frequency-dependent dielectric tensors as well as related quantities like reflectivities, absorption coefficients, optical conductivities, energy loss functions, refractive indices, and extinction coefficients. The optical anisotropy in this mate-rial, manifested in the infinity-frequency dielectric constant, low-frequency refractive index, and the effective number of electrons participating in the interband transitions along the principal axes was clearly revealed in our calculations. The reflectivity spectra obtained from our calculations, as well as by Jiang, Xu, and Ching[24] predicts large reflectivity in the low-energy spectra when the electric field is parallel to the **c** axis. The optical spectra obtained for the antiferroelectric phase is almost the same as that of the ferroelectric phase, indicating that the discrepancy between experimental and theoretical results in $\mathbf{E}\|\mathbf{c}$ is not due to antiferroelectric dis-tortion. More experimental studies at the lower-energy range are required to confirm our observations.

*Electronic address: P.Ravindran@fysik.uu.se

[1] S. Sawada, S. Nomura, S. Fuji, and I. Yoshida, Phys. Rev. Lett. **1**, 320 (1958).

[2] M. I. Kay, J. A. Gonzalo, and R. Maglic, Ferroelectrics **9**, 179 (1975); F. Ramondo, Chem. Phys. Lett. **156**, 346 (1989).

[3] K. S. Kam and J. H. Henkel, Phys. Rev. B **17**, 1361 (1978).

[4] J. T. Leong and R. M. Emrick, J. Phys. Chem. Solids **32**, 2593 (1971).

[5] I. Hatta, Y. Shimizu, and K. Hamano, J. Phys. Soc. Jpn. **44**, 1887 (1978); V. V. Lemanov, Ferroelectrics **78**, 163 (1988).

[6] S. A. Ahmed and M. H. Ali, Phys. Status Solidi B **194**, 517 (1996).

[7] M. Kamada and R. Kato, J. Phys. Soc. Jpn. **45**, 169 (1978); W. Dietrich, L. Schmid, and D. Schmid, Chem. Phys. Lett. **28**, 249 (1974).

[8] C. M. Hartwig, E. Wiener-Avnear, and S. P. S. Porto, Phys. Rev. B **5**, 79 (1972); R. M. Hazen and L. W. Finger, J. Appl. Phys. **50**, 6826 (1979); I. Hatta, Y. Shimizu, and K. Hamano, J. Phys. Soc. Jpn. **44**, 1887 (1978).

[9] K. Inoue, Ferroelectrics **7**, 107 (1974); H. Vogt, J. Appl. Phys. **5**, 85 (1974).

[10] S. Singh and K. Singh, J. Phys. Soc. Jpn. **36**, 1588 (1974).

[11] S. V. Pan'kova, V. V. Poborchii, and V. G. Solov'ev, J. Phys.: Condens. Matter **8**, L203 (1996).

[12] K. Ema, K. Hamano, and I. Hatta, J. Phys. Soc. Jpn. **39**, 726 (1975).

[13] J. D. Axe, Phys. Rev. **167**, 573 (1968).

[14] T. Yanagi and S. Sawada, J. Phys. Soc. Jpn. **25**, 799 (1968).

[15] H. Yamashita and R. Kato, J. Phys. Soc. Jpn. **29**, 1557 (1970).

[16] M. Kamada and R. Kato, J. Phys. Soc. Jpn. **45**, 169 (1978).

[17] H. Kawaura, Y. Kawaguchi, and R. Kato, J. Phys. Soc. Jpn. **57**, 3613 (1988).

[18] B. Wyncke, F. Bréhat, and H. Kharoubi, J. Phys.: Condens. Matter **2**, 8791 (1990).

[19] K. Wu and C. Chen, Chem. Phys. Lett. **196**, 62 (1992).

[20] A. M. El-Dib and H. F. Hassan, Phys. Status Solidi **25**, 249 (1967).

[21] D. Kucharczyk, A. Pietraszko, and K. Lukaszewicz, Phys. Status Solidi A **37**, 287 (1976).

[22] M. I. Kay, Ferroelectrics **4**, 235 (1972).

[23] M. I. Kay and B. C. Frazer, Acta Crystallogr. **14**, 56 (1961).

[24] H. Jiang, Y.-N. Xu, and W. Y. Ching, Ferroelectrics **136**, 137 (1992).

[25] X. F. Zhong, H. Jiang, and W. Y. Ching, Ferroelectrics **153**, 31 (1994).

[26] M. Ashida, O. Ohta, M. Kamada, M. Watanabe, and R. Kaot, J. Electron Spectrosc. Relat. Phenom. **79**, 55 (1996).

[27] G. E. Ziegler, Phys. Rev. **38**, 1040 (1931).

[28] M. I. Kay, Ferroelectrics **4**, 235 (1972).

[29] G. B. Carpenter, Acta Crystallogr. **5**, 132 (1952).

[30] Y. Yamada, I. Shibuya, and S. Hoshino, J. Phys. Soc. Jpn. **18**, 1594 (1963); Y. Yamada and T. Yamada, *ibid.* **21**, 2167 (1966).

[31] J. M. Wills (unpublished); J. M. Wills and B. R. Cooper, Phys. Rev. B **36**, 3809 (1987); D. L. Price and B. R. Cooper, *ibid.* **39**, 4945 (1989).

[32] O. K. Andersen, Phys. Rev. B **12**, 3060 (1975); O. K. Andersen

and O. Jepsen, Phys. Rev. Lett. **53**, 2571 (1984); O. K. Andersen, O. Jepsen, and D. Glötzel, in *Highlights of Condensed-Matter Theory*, edited by F. Bassani, F. Fumi, and M. P. Tosi (North-Holland, New York, 1985); W. R. L. Lambrecht and O. K. Andersen, Phys. Rev. B **34**, 2439 (1986); H. Skriver, *The LMTO Method* (Springer, Berlin, 1984).

[33] L. Hedin and B. I. Lundquist, J. Phys. C **1**, 2064 (1971).

[34] D. J. Chadi and M. L. Cohen, Phys. Rev. B **8**, 5747 (1973); H. J. Monkhorst and J. D. Pack, *ibid.* **13**, 5188 (1976); S. Froyen, *ibid.* **39**, 3168 (1989).

[35] H. Ehrenreich and M. H. Cohen, Phys. Rev. **115**, 786 (1959).

[36] M. Alouani and J. M. Wills, Phys. Rev. B **54**, 2480 (1996); R. Ahuja, S. Auluck, J. M. Wills, M. Alouani, B. Johansson, and O. Eriksson, *ibid.* **55**, 4999 (1997).

[37] K. A. Verkhovskaya and A. S. Sonin, Zh. Eksp. Teor. Fiz. **52**, 387 (1967) [Sov. Phys. JETP **25,** 249 (1967)].

[38] J. W. Sidman, J. Am. Chem. Soc. **79**, 2669 (1957).

[39] M. Kamada, K. Ichikawa, and K. Tsutsumi, J. Phys. Soc. Jpn. **50**, 170 (1981).

[40] R. M. Hazen and L. W. Finger, J. Appl. Phys. **50**, 6826 (1979).

[41] R. W. G. Wyckoff, *Crystal Structures,* 2nd ed. (Wiley, New York, 1954), Vol. I.

[42] M. Okuda, S. Ohba, Y. Saito, T. Ito, and I. Shibya, Acta Crystallogr., Sect. B: Struct. Sci. **46**, 343 (1990).

[43] R. Newman, J. Chem. Phys. **20**, 444 (1951).

[44] V. Bellani, G. Guizzetti, F. Marabelli, A. Piaggi, A. Borghesi, F. Nava, V. N. Antonov, VI. N. Antonov, O. Jepsen, O. K. Andersen, and V. V. Nemoshkalenko, Phys. Rev. B **46**, 9380 (1992).

[45] M. Kamada, M. Yoshikawa, and R. Kato, J. Phys. Soc. Jpn. **39**, 1004 (1975).

[46] M. K. Barnoski and J. M. Ballantyne, Phys. Rev. **174**, 946 (1968); C. M. Hartwig, E. Wiener-Avnear, and S. P. S. Porto, Phys. Rev. B **5**, 79 (1972).

[47] L. McEwen, J. Chem. Phys. **21**, 319 (1953).

[48] S. Logothetidis and G. Kiriakidis, J. Appl. Phys. **64**, 2391 (1988).